ChemPubSoc Europe

DOI: 10.1002/chem.201501170

CHEMISTRY A European Journal Full Paper

Hydrogels |*Hot Paper*|

Phenylboronic Acid Appended Pyrene-Based Low-Molecular-Weight Injectable Hydrogel: Glucose-Stimulated Insulin Release

Deep Mandal, Subhra Kanti Mandal, Moumita Ghosh, and Prasanta Kumar Das*[a]

Abstract: A pyrene-containing phenylboronic acid (PBA) functionalized low-molecular-weight hydrogelator was synthesized with the aim to develop glucose-sensitive insulin release. The gelator showed the solvent imbibing ability in aqueous buffer solutions of pH values, ranging from 8–12, whereas the sodium salt of the gelator formed a hydrogel at physiological pH 7.4 with a minimum gelation concentration (MGC) of 5 mg mL^{-1}. The aggregation behavior of this thermoreversible hydrogel was studied by using microscopic and spectroscopic techniques, including transmission electron microscopy, FTIR, UV/Vis, luminescence, and CD spectroscopy. These investigations revealed that hydrogen bonding, π–π stacking, and van der Waals interactions are the key factors for the self-assembled gelation. The diol-sensitive PBA part and the pyrene unit in the gelator were judiciously used in fluorimetric sensing of minute amounts of glucose at physiological pH. The morphological change of the gel due to addition of glucose was investigated by scanning electron microscopy, which denoted the glucose-responsive swelling of the hydrogel. A rheological study indicated the loss of the rigidity of the native gel in the presence of glucose. Hence, the glucose-induced swelling of the hydrogel was exploited in the controlled release of insulin from the hydrogel. The insulin-loaded hydrogel showed thixotropic self-recovery property, which hoisted it as an injectable soft composite. Encouragingly, the gelator was found to be compatible with HeLa cells.

Introduction

In the twenty first century, diabetes is one of the most common chronic disorders associated with glucose. In human body, insulin carries glucose from food to cells.[1] In type 1 diabetes the insulin production from the pancreas is hampered, ensuing a high glucose level in the bloodstream.[2] Consequently, external insulin needs to be injected to sustain a proper blood glucose level. Glucose responsive materials have significant potential in the advancement of the insulin regulatory systems that are needed for hyperglycemic therapies.[3,4] In this perspective, a glucose-stimulated release of insulin from soft materials (e.g., gels, vesicles, etc.) is a subject of huge importance. In recent times, there is a growing impetus in the development of stimuli-responsive gels that undergo physicochemical changes in response to external stimuli such as pH value, temperature, ionic strengths, biomolecules, and so on.[5–7] These unique properties of gels were comprehensively employed in molecular recognition, sensors, actuators, drug delivery, and other domains.[3,4,8–11] The stimuli sensitivity can be developed in the gelator scaffold by introducing task specific functionalities.

In this regard, phenylboronic acid (PBA) is known to be an intelligent saccharide receptor due to its unique ability to form reversible covalent bonds with diols.[12] Most of the reported PBA derivatives demonstrate glucose sensitivity primarily based on fluorescent detection in solution phase at alkaline pH values (i.e., pH 8–12).[13,14] To this end, James and coworkers had reported a variety of boronic acid based molecular receptors for selective saccharide sensing in an aqueous methanolic buffer of pH 8.2 and a carbonate buffer of pH 10.[15,16] However, none of the reported molecules are capable of forming a self-assembled hydrogel. There are reports on glucose-responsive polymeric gels that regulate either chemically modified insulin or release insulin at higher pH-value ranges (i.e., pH 8.5–10).[17,18] In comparison to polymeric gels, low-molecular-weight gels (LMWGs) could be more befitting as they are reversible in nature and more sensitive to the changes of their adjacent environment.[19] In addition, if the insulin regulatory low-molecular-weight gels can be made to be injectable through its thixotropic property, it would be highly befitting in

[a] *D. Mandal, S. K. Mandal, M. Ghosh, Prof. P. K. Das*
Department of Biological Chemistry
Indian Association for the Cultivation of Science
Jadavpur, Kolkata, 700032 (India)
E-mail: bcpkd@iacs.res.in

*Supporting Information for this article is available on the WWW under http://dx.doi.org/10.1002/chem.201501170. It contains a table for the MGCs of compound **1** at different pH values, a representation of I/I_0 versus glucose concentration at different peaks, a synthetic scheme, the ^{1}H NMR spectroscopic and mass spectrometric analysis of compounds **1** and **1a**, UV/Vis spectra of compound **1a**, the quenching of fluorescence through PET due to incorporation of PBA group, ^{1}H NMR spectra of compound **1a** with the glucose-containing supernatant solution on top of the gel, fluorescence spectra of the glucose-containing supernatant solution, a calibration curve of gelator **1a**, photographs of gel **1a** irradiated with a UV torch in the absence and presence of glucose after swelling, an absorption spectrum of standard insulin, a calibration curve of insulin, the step-strain time-dependent rheological analysis, and a fluorescence micrograph of the HeLa cells in the presence of compound **1a**.*

treating diabetic patients. Till date, no low-molecular-weight hydrogel has been reported that demonstrates glucose sensing as well as glucose-stimulated release of insulin at physiological pH. Hence, we aim to design a glucose-sensitive injectable LMHG that can detect minute amount of glucose at physiological pH and subsequently can be used as glucose-stimulated insulin regulatory vehicle. There are several detection methods for monitoring the saccharide content including UV/Vis absorbance, fluorescence, circular dichroism, electrochemistry, equilibrium dialysis, Raman spectroscopy, nuclear magnetic resonance spectroscopy, holographic detection, and others.[20–22] Among these techniques, one of the most prominent and powerful optical read out for saccharide sensing is fluorescent detection as it deals with very minute analyte concentrations and excellent sensitivity.[20] Thus, the development of a fluorescent LMHG with a glyco-responsive PBA functionality would be helpful for the fluorimetric detection of glucose.

In the present study, we developed the pyrene-containing PBA-functionalized low-molecular-weight hydrogelator **1** (Figure 1 A) that can form a gel in aqueous buffer of pH values ranging from 8–12. The sodium salt of the gelator, that is, compound **1 a**, showed an efficient hydrogelation ability in a phosphate-buffered saline (PBS) solution of pH 7.4. Interestingly, compound **1 a** can sense minute amount of glucose (0.1 mM) at physiological pH (i.e., pH 7.4) through fluorescence detection. Upon addition of glucose (0.1–0.6 mM), the intrinsic fluorescent intensity of the gelator was enhanced twofold. Importantly, the gel fibers swelled with an increase in the fiber size in the presence of glucose. The loosening of the fibrillar network owing to the swelling of this LMHG in the presence of glucose, assisted in the controlled release of insulin entrapped within the self-assembled fibrillar network (SAFIN) of the hydrogel. The most advantageous property of the insulin-loaded hydrogel **1 a** was its thixotropic self-recovery property. This unique thixotropic property of the gel–insulin composite made it injectable and hoisted an opportunity to use it in diabetic treatment. Moreover, the newly developed hydrogelator **1 a** was found to be highly compatible towards HeLa cells, which essentially enhanced its potential applications in biomedicine.

Results and Discussion

The development of soft material (such as gels, vesicles, etc.) based insulin regulatory vehicle that can simultaneously recognize glucose and release insulin in response to an external glucose stimuli is in high demand. Moreover, the development of such stimuli-responsive soft materials with sufficient bio-compatibility is a challenging task particularly when we envisage its applications in biomedicine including hyperglycemic therapies. LMHGs comprised of fluorophore-tagged glyco-sensitive motifs could be suitable to achieve the said objective. The essential parameter that in general influence the self-assembled gelation are hydrophobic interactions, π–π stacking, hydrogen bonding, and most importantly, the optimum hydrophilic–lipophilic balance (HLB) in the gelator scaffold.[23–31] Considering these factors, gelator **1** (Figure 1 A) was synthesized with a pyrene moiety coupled with phenylboronic acid by an amino acid (L-phenylalanine) and a 2,2′-(ethylenedioxy)bis(ethylamine) linker (Scheme S1 in the Supporting Information). The aromaticity of the pyrene is expected to provide the necessary π–π stacking and hydrophobic interaction required for self-assembled gelation.[25] Intermolecular hydrogen bonding originated from amide bonds of the amino acid linker might help in self-aggregation.[25] The ethyleneoxy spacer was integrated mainly to provide the necessary hydrophilicity in the gelator backbone. Aryl boronates have an intrinsic affinity towards dihydroxyl groups (such as glucose), which is helpful in the development of glucose sensors. Earlier study reported that boronic acid is a sufficiently biocompatible group with low immunogenicity.[32] Hence, PBA was included at the terminal position to bring in glycosensitivity and hydrophilicity in the structure of the gelator.

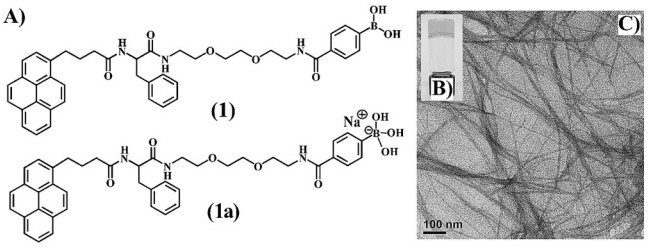

Figure 1. A) Structure of the investigated hydrogelators. B) Photograph of the hydrogel. C) TEM image of the hydrogel **1 a**.

Gelation behavior and characterization of the hydrogel

Compound **1** showed the gelation ability in aqueous buffer solution of varying pH values (i.e., pH 8.5–12.0, carbonate buffer) with the minimum gelation concentrations (MGCs) of 3.7–6.6 mg mL^{-1} (Table S1 in the Supporting Information). However, compound **1** could not form a hydrogel at physiological pH (i.e., pH 7.4). Notably, the Na salt of compound **1**, that is, compound **1 a**, showed efficient hydrogelation in 25 mM phosphate buffer at pH 7.4 (yellow colored gel, Figure 1 B) having a MGC of 5 mg mL^{-1}. Hydrogels formed at different pH values were thermoreversible in nature, which means that they melted by slow heating and again turned to gel on cooling. The gels were stable at room temperature for several months. The temperature at which the gel converts into a solution is referred to as gel melting temperature or gel-to-sol transition temperature (T_{gel}).[25] In the case for the LMHG **1 a**, the T_{gel} was recorded to be 68 °C at the MGC (i.e., 5 mg mL^{-1}). Considering the envisaged applications of the hydrogel in glucose sensing and insulin release, our study mainly deals with the LMHG **1 a** as it can form a gel at the physiologically relevant pH value (i.e., pH 7.4).

The morphological and physicochemical properties of the hydrogel **1 a** were investigated by microscopic and spectroscopic techniques. A transmission electron microscopic (TEM) image of the dried hydrogel confirmed the formation of an entangled fibrillar network of compound **1 a**. The gel fibers had an average diameter of 15–20 nm with a length of several micrometers (Figure 1 C). The influence of different non-covalent

interactions operating in the self-aggregation of the gelators was investigated by using FTIR spectroscopy. FTIR spectra were recorded for compound **1a** in the non-self-assembled state in chloroform ($CHCl_3$) as well as in the gel state in D_2O (Figure 2A). The FTIR spectra of compound **1a** in the non-gelating solvent $CHCl_3$ showed the transmittance peaks at approximately $\tilde{\nu}=3312$, 1641, and 1509 cm^{-1} that were originated due to

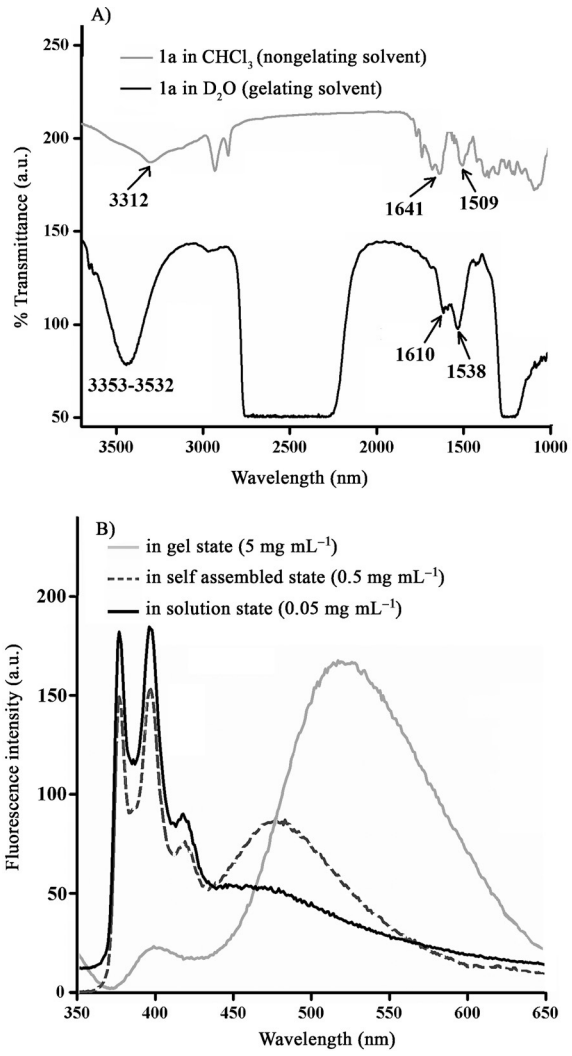

Figure 2. A) FTIR spectra of compound **1a** in $CHCl_3$. B) Fluorescence spectra of compound **1a** with varying concentrations.

ν_{N-H} (amide A), amide $\nu_{C=O}$ (amide I), and ν_{N-H} (amide II) vibrations, respectively. These peaks were shifted to approximately $\tilde{\nu}=3353$–3532 (broad band), 1610, and 1538 cm^{-1}, respectively, upon gelation in D_2O. This shift in the stretching and bending frequencies suggests the involvement of intermolecular hydrogen bonding between carbonyl and amide NH groups during the self-assembled gelation.[25] According to the UV/Vis spectra of compound **1a**, a bathochromic shift was noted when the solvent was moved from the non-gelating $CHCl_3$ to a gelating one (i.e., PBS solution) (Figure S1 in the Supporting Information). It is characteristic for a J-type aggregation, which had taken place during the self-assembly of compound **1a** in aqueous buffer. The aggregates that exhibit bathochormically shifted J-band in their absorption spectrum, are called J-aggregates.[33,34] It was originated due to edge-by-edge or side-to-side assemblies.

Fluorescent spectroscopy is another important technique to study the molecular interactions in self-assembled gelation. The fluorescence spectra of compound **1a** at very low concentration (0.05 mg mL^{-1}, i.e., 100 times lower than the MGC), showed a strong emission peak at $\lambda=396$ nm along with two other peaks at $\lambda=376$ and 417 nm upon excitation at $\lambda=340$ nm (Figure 2B). The characteristic of the emission spectrum, which is akin to the molecular pyrene, indicates that the gelator molecule is in its non-self-assembled state at the experimental concentration. With increase in the gelator concentration to 0.5 mg mL^{-1} a new excimer peak generated at a higher wavelength ($\lambda=476$ nm). At the MGC (5 mg mL^{-1}) the fluorescence intensity of the excimer peak significantly enhanced and further red shifted to $\lambda=519$ nm. The emission intensity, due to the molecular pyrene of compound **1a**, substantially decreased with an increase in the gelator concentration. The appearance of the excimer peak indicates the participation of π–π interaction between the adjacent pyrenyl moieties during the self-assembly of compound **1a**.[15,25] The generation of the excimer peak at a concentration of approximately 0.5 mg mL^{-1} also pointed out that the self-assembly process might have been initiated around this concentration. With further increase in the gelator concentration, the intensity of the excimer peak notably enhanced due to the participation of more gelators in the self-aggregation that led to an enhancement in the π–π interactions between the pyrenyl groups. Consequently, the fraction of non-self-assembled molecules decreased, which resulted in a drastic drop in the emission peak intensity of molecular pyrene.

Circular dichroism (CD) spectroscopy provides information about the nature of the supramolecular aggregation depending on the molecular structures of the gelators. The CD spectra of compound **1a** have a negative cotton effect with double minima at $\lambda=218$ and 240 nm (Figure 3A). The peaks became more prominent with an increase in the concentration of compound **1a**. The double minima in the CD spectra denote an α-helical nature of the supramolecular chiral aggregates (not by the positions but by its pattern).[25] From temperature-dependent CD spectra it was observed that the CD peaks lost their intensity with a rise in temperature up to 80 °C. Notably, the peak intensities were regained upon cooling back to 20 °C (Figure 3B).

Hence, the hydrophobic and π–π interactions originated from the pyrenyl moiety, the intermolecular hydrogen bonding between the amide linkage, and possibly the required HLB attained by the presence of the hydrophilic boronic acid aided the self-assembled hydrogelation of the PBA-tethered gelator, **1a**.

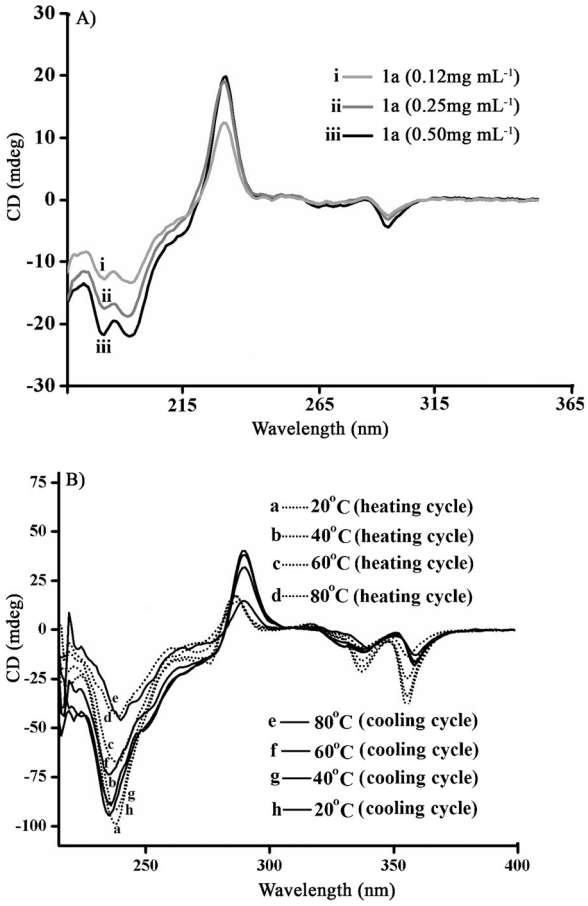

Figure 3. A) Concentration-dependent CD spectra of compound **1 a**. B) Temperature-dependent CD spectra of compound **1 a** (1 mg mL^{-1}).

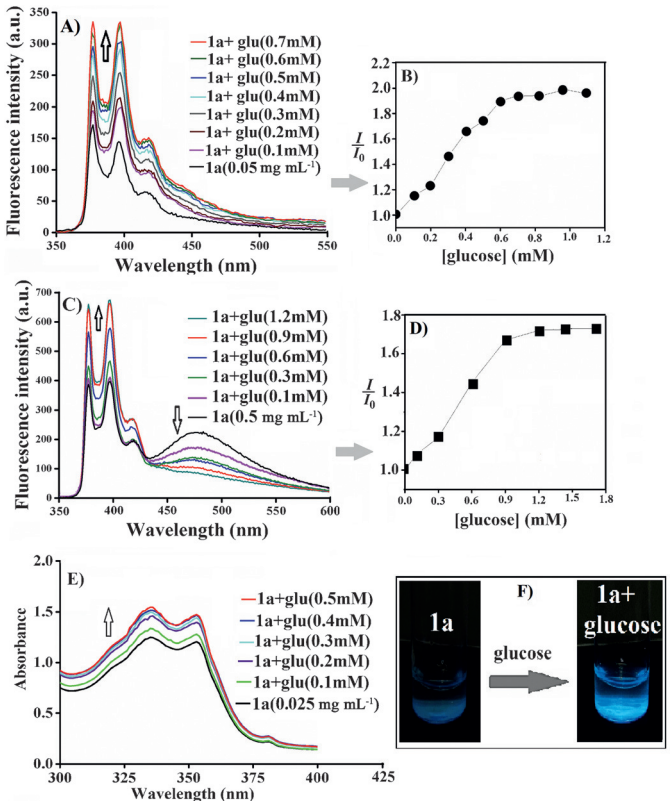

Figure 4. A) and C) Fluorescence spectra of compound **1 a** at different concentrations (A = 0.05 and C = 0.5 mg mL^{-1}) with increasing glucose (glu) concentration. B) and D) Correlation curves (I/I_0 vs. glucose concentration) for the incremental change in the peak intensity at $\lambda = 376$ nm with fixed gelator concentration of 0.05 (B) and 0.5 mg mL^{-1} (D). E) UV/Vis spectra of compound **1 a** with varying glucose concentration. F) Photographs of a solution of compound **1 a** in the absence and presence of glucose upon irradiating with a UV torch.

Glucose sensing

At this point, we wanted to make use of the PBA linked at the terminal of gelator **1 a** for glucose sensing. The intrinsic fluorescent character of the pyrene moiety in the gelator was utilized for the fluorimetric detection of D-glucose. Fluorescence spectra of compound **1 a** (0.05 mg mL^{-1}, at the non-self-assembled state) showed that the emission intensity of the pyrene notably enhanced with the addition of very little amount of glucose (0.1 mM, Figure 4 A). The emission intensity of the gelator steadily increased with an increase of the glucose concentration. The maximum improvement was two-fold at 0.6 mM and became saturated with further increase of the glucose concentration. Importantly, minute amount of glucose can be easily sensed through fluorescence detection by this newly developed gelator **1 a** at very low concentration. At the self-aggregated state of compound **1 a** (0.5 mg mL^{-1}), the intensity of the excimer peak at $\lambda = 476$ nm gradually decreased, whereas the molecular emission peak intensity (at $\lambda = 376$ and 417 nm) owing to the pyrene moiety steadily improved with an increase of the glucose concentration from 0.1 to 1.2 mM (Figure 4 C). The highest incremental change in the fluorescence intensity was noted for the peak appeared at $\lambda = 376$ nm. A correlation between the fluorescent intensity (I/I_0 vs. glucose concentration, where I_0 = fluorescence intensity of compound **1 a** in the absence of glucose, I = fluorescence intensity of compound **1 a** in the presence of varying glucose concentrations) of the peak appeared at $\lambda = 376$ nm and the glucose concentration was given for a gelator concentration of 0.5 and 0.05 mg mL^{-1} (Figures 4 B and D). A continuous enhancement in the emission intensity profile was noted with an increase of the glucose concentration. Also a correlation table was drawn to compare the highest increment in peak intensity (I/I_0) at different peaks (i.e., $\lambda = 376$, 417, and 476 nm, Table S2 in the Supporting Information) at different glucose concentrations. In the UV/Vis spectra of the gelator **1 a** (0.025 mg mL^{-1}), the absorbance intensity of the pyrene gradually enhanced (Figure 4 E) with an increase of the amount of glucose (0.1–0.5 mM). Even the change in the bright blue fluorescence of compound **1 a** in the absence and presence of glucose can be differentiated when the solution is irradiated with a UV torch (Figure 4 F). The presence of glucose can be easily sensed visually from the bright fluorescence of the gelator compared to that of the native gel. Besides glucose, other saccharides like galactose and fructose that are present in blood may also interfere with the fluorescence property of compound **1 a**. Surprisingly, we found an almost unaltered fluorescence behavior of the gelator **1 a** upon addition of galactose up to 15 mM.

The fluorescence intensity of compound **1a** merely enhanced by 1.2-fold in the presence of 10 mM D-fructose. Thus, the sensitivity of gelator **1a** towards galactose and fructose is very poor. Moreover, the concentrations of galactose and fructose in blood are too low (0.1 mM) to interfere with the glucose sensing by the fluorescence property of compound **1a**.[43]

The probable reason behind the enhanced emission intensity of compound **1a** in the presence of glucose could be as follows. In aqueous medium, the PBA-tethered gelator remains in equilibrium with its neutral/trigonal from (i.e., compound **1**) and the anionic/tetrahedral form (i.e., compound **1a**) (Scheme 1).[20,35–37] The direction of the equilibrium depends on

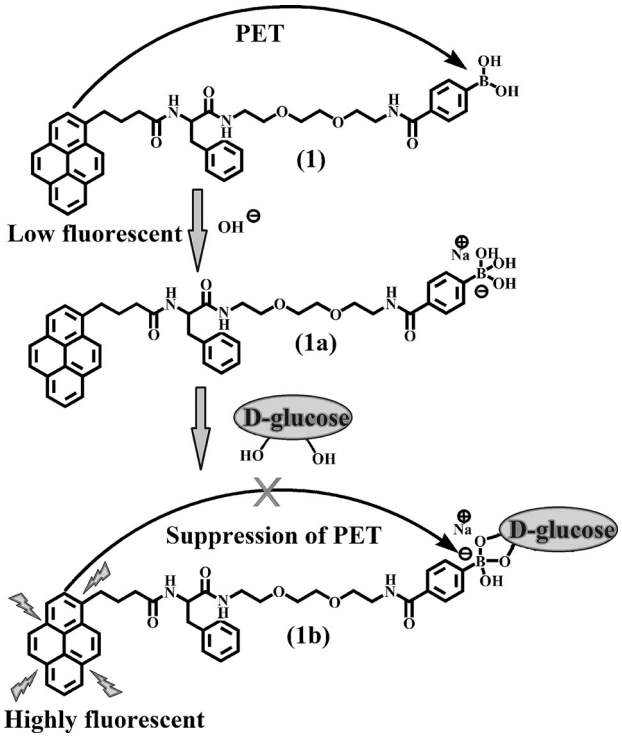

Scheme 1. Schematic representation of the PET process and the fluorescence enhancement of the gelator upon addition of glucose through the suppression of the PET.

the pK_a value of PBA and the pH value of the solution. The pK_a value of PBA is approximately 8.9, which get reduced to approximately 8.0 upon linking up with an electron-withdrawing group like amide.[36,37] At physiological pH (i.e., pH 7.4), there will be an equilibrium between the two forms (i.e., compounds **1** and **1a**) with a shift towards the neutral/trigonal boronic acid form **1**. The sp^2-hybridized boron atom in neutral boronic acid (i.e., compound **1**) behaves as an electron-acceptor moiety.[20,38] Excitation of the gelator at $\lambda = 340$ nm, possibly led to a photoinduced electron transfer (PET) between the excited pyrene donor to the boron acceptor. To understand the PET quenching of the pyrene due to the presence of PBA, we have performed a fluorescence experiment of the gelator moiety before (compound **vi** in Scheme S1 in the Supporting Information) and after covalently attaching the PBA group (compound **1a**) in a DMSO/water (1:3, v/v) mixture. We found that the emission intensity of the pyrene moiety (compound **vi**) was notably decreased when the PBA group was covalently attached to it (resulting in compound **1a**) (Figure S2 in the Supporting Information). Hence, it can be affirmed that the molecular emission behavior of pyrene gets suppressed owing to this PET process (Scheme 1) resulting in low fluorescence. In presence of glucose, compound **1a** forms a cyclic boronate-1,2-diol adduct (compound **1b**, Scheme 1) where the overall equilibrium is shifted to the stable anionic boronate ester form (Scheme 1). The sp^3-hybridizes boron atom of compound **1b** can no longer serve as an electron-acceptor atom. This transformation of the boron atom from sp^2 to sp^3 obviously weakens the PET process and consequently, a notable enhancement in the fluorescence intensity of pyrene in both molecular and self-assembled state was noted (Figures 4A and C).[20,35,38] Moreover, in the presence of glucose the overall HLB of the gelator **1b** might have been altered, which would affect the nature of self-aggregation. The altered HLB might have hindered the π–π stacking interaction between the pyrene moieties. As a result, the excimer peak (Figure 4C) that appeared at the self-aggregated state of compound **1a** (0.5 mg mL^{-1}) was gradually decreased with an increase of the glucose concentration.

At this point, we were intrigued to find out the morphological changes taking place to the self-assembled fibrillar network (SAFIN) of the LMHG upon addition of glucose. According to a scanning electron microscopic (SEM) study, the images showed that the native gel had a fiber diameter of 15–20 nm (Figure 5A). The fiber diameters gradually increased up to 40–50, 58–70, and 80–120 nm in presence of 6, 12, and 18 mM glucose, respectively for compound **1b** (Figures 5B–D). These size expansions of the gel fibers strongly support a glucose-induced swelling behavior of the gel (Figure 5E). Presumably, the addition of glucose altered the nature of the self-assembly and resulted in the swelling of the hydrogel. The degree of swelling (or mass swelling) is the most important parameter in swelling studies. The percentage degree of swelling (% DS) was calculated from the following Equation (1):

$$\%\,\mathrm{DS} = (M_t - M_0)\,100\,M_0 \qquad (1)$$

where M_t is the mass in [mg] of the swollen gel at a time t and M_0 is the mass in [g] of the initial xerogel.[39] According to the Figure 5F, it was clearly understood that the degree of swelling gradually enhanced with time and became saturated when it attained equilibrium swelling condition. This increment in % DS was found to be more prominent with an increase of the glucose concentration (6, 12, and 18 mM) compared to PBS solution of pH 7.4.

At this instant, there could be a possibility of gel dissolution/dilution due to the addition of aqueous buffer/glucose solution on top of the gel during the swelling of the gel. To investigate this issue, we have carried out ^{1}H NMR, fluorescence, and UV absorption spectroscopy experiments (Figures S3, S4, and S5 in the Supporting Information respectively) of the supernatant solution containing 18 mM glucose (on top of the

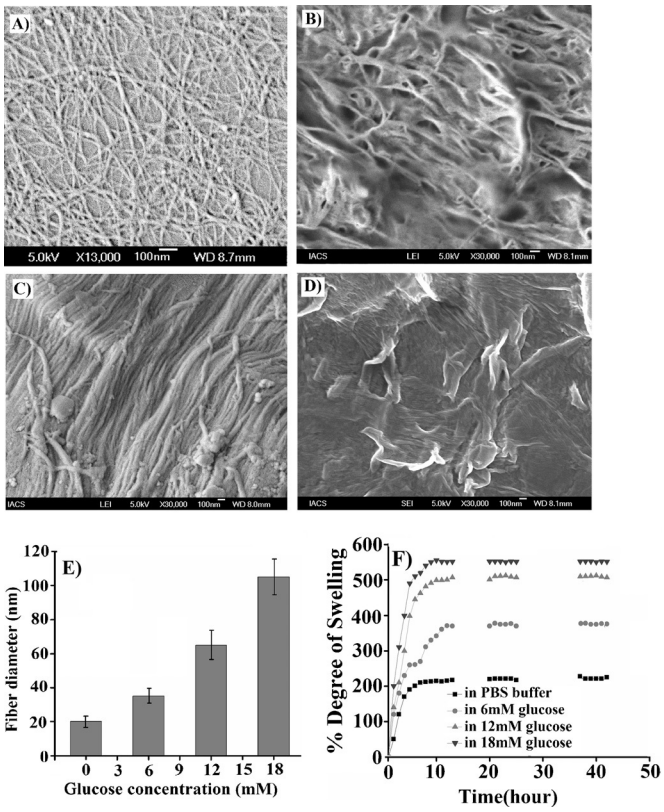

Figure 5. SEM images of compound **1 a** in the presence of different glucose concentration: A) 0, B) 6, C) 12, and D) 18 mM. E) Plot of the average gel fiber diameters at different glucose concentrations. F) Plot of the % degree of swelling with time at different glucose concentrations.

gel). In the ^{1}H NMR experiment after 24 h of incubation no detectable signal of the gelator was observed in the NMR spectra of the supernatant solution in D_2O (Figure S3 in the Supporting Information). Similarly, in the fluorescence spectroscopic experiment very poor intensity of compound **1 a** was observed (Figure S4 in the Supporting Information) between 6 and 24 h of the gel swelling experiment. The observed fluorescence intensity of compound **1 a** in the supernatant solution is remarkably lower compared to that of the gel. The amount of gelator coming out through dissolution was quantified by UV/Vis absorption by using a standard calibration curve (Figure S5 in the Supporting Information). An amount of 1 mL of PBS solution (pH 7.4) and 18 mM glucose solution was poured separately over 1 mL of the gel at the MGC (5 mg mL^{-1}). After 24 h, the absorbance value of the supernatant solution was recorded at $\lambda = 340$ nm and the concentrations of the dissolved compound **1 a** were found to be only 0.015 and 0.024 mg mL^{-1}, respectively. This indicated that only 0.42–0.5% of the initial gelator amount was lost due to dissolution during swelling, which is insignificant with respect to the gel at the MGC (5 mg mL^{-1}). We have irradiated the filtered gel with a UV torch after the swelling experiment (Figure S6 in the Supporting Information). Here too notable enhancement of fluorescence of the swelled gel was observed, whereas the fluorescence intensity of the supernatant glucose solution (Figure S4 in the Supporting Information) was unaltered.

Rheological behavior

Now, it would be intriguing to find out how the stiffness of the gel changed upon addition of glucose to the soft materials. Rheological studies provide information on the fluidity and rigidity of viscoelastic materials such as gels. Two major parameters related to the viscoelasticity are the storage modulus (G') and the loss modulus (G''). The storage modulus G' refers to the ability of a deformed material to restore its native form whereas the loss modulus G'' represents the flow behavior of the material under applied stress. For viscoelastic materials like gels $G' > G''$ (G' and $G'' \approx \omega^0$, $\omega =$ angular frequency), and in the sol state $G'' > G'$ ($G' \approx \omega^2$ and $G'' \approx \omega$).[24–26] The stiffness of the LMHG **1 a** in the absence and presence of glucose was determined from a rheological study (Figure 6). In a typical oscillatory frequency sweep experiment of the native LMHG **1 a** (5 mg mL^{-1}) at a fixed strain (γ, 0.01%), the storage modulus

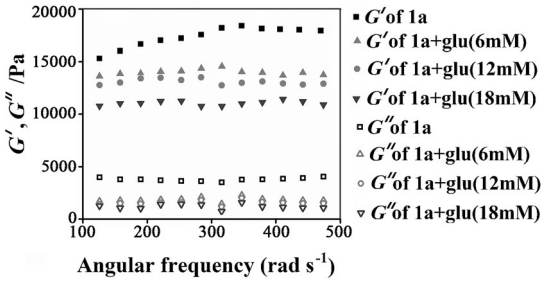

Figure 6. Rheology of compound **1 a** (5 mg mL^{-1}) with increasing glucose (glu) concentrations.

($G' \approx 17\,000$ Pa) was noted to be higher than the loss modulus ($G'' \approx 4000$ Pa) over the entire angular frequency. This is a typical characteristic of a viscoelastic material. Surprisingly, addition of glucose to the gel causes reduction in the G' value. In the presence of a 6 mM glucose solution the G' value was reduced to approximately 14 000 Pa for gel **1 a** (5 mg mL^{-1}). With an increase of the glucose content (12 and 18 mM), the G' value further decreased to 13 200 and 11 000 Pa, respectively. This gradual decrease of the G' value with an increasing glucose concentration clearly indicates the weakening of the stiffness of the gel. The decrease of the stiffness of the gluconated gel **1 a**, probably originated from the change in the packing of the fibers or the change in the charged environment of the fibers upon binding with glucose. The decrease of the stiffness might also be a consequence of the glucose-triggered swelling of the gel.

Glucose-stimulated release of insulin from the hydrogel

Hydrogels are finding significant promise as drug delivery vehicle.[40,41] The interstitial space within the fibrillar network of the hydrogel might help in the entrapment of a drug and release it at a rate, which is dependent on the porosity of the hydrogel correlated to the extent of the crosslinked SAFIN.[40,41] Hence, drug diffusion is supposed to be tuned by the degree of swel-

ling of the hydrogel. To this end, glucose-stimulated swelling of the LMHG **1a** (as observed from our SEM study), encouraged us to explore its possible application for in vitro drug release through a diffusion pathway.[40,41] Insulin was loaded within the LMHG **1a** at pH 7.4. Maximum 0.138 mg mL^{-1} of insulin can be loaded within the SAFIN without disconcerting the stability of the gel at the MGC (5 mg mL^{-1}). The drug loading capacity of the hydrogeln**1a** can be improved by increasing the gelator concentration. Insulin (0.05 mg mL^{-1}) loaded hydrogel (5 mg mL^{-1}, MGC) composites were used to investigate the glucose-stimulated release of insulin. The amount of released insulin was estimated from the absorbance value of the supernatant solution at $\lambda = 276$ nm (Figures S7 and S8 in the Supporting Information).[42] In the presence of only PBS solution (pH 7.4) the insulin diffusion from the SAFIN was merely 13% within 24 h. Aqueous glucose solutions (600 μL) of varying concentrations (6, 12, and 18 mM) were added on the top of each preloaded insulin–hydrogel (**1a**) composite and incubated for several hours. The amount of released insulin increased with an increase in time and after 24 h it was recorded to be approximately 35 and about 58% in the presence of 6 and 12 mM glucose, respectively (Figure 7A). The insulin release from the hydrogel network accelerated at higher concentration of glucose. Almost 80% of the insulin were released in 24 h in the presence of 18 mM glucose. Release of insulin entrapped within the SAFIN through diffusion might be a consequence of the glucose-induced swelling of the hydrogel. The change in the electrical microenvironment of the fibers due to addition of glucose might also be a driving force behind the release of entrapped materials. The insulin release proportionately increased as the degree of swelling improved with an increase of the glucose concentration.[43–46] Hence, the rate of insulin diffusion from the hydrogel can be tuned by varying the glucose concentration. Generally, the human body contains plasma glucose concentrations of approximately 5.5–6.0 mM, whereas for diabetic patients it is above 10 mM.[43] Interestingly, at higher glucose concentration (i.e., above 10 mM), compound **1a** can release high amount of drug (58-80%, depending on the glucose concentrations). This regulatory release of insulin could be well-suited with the needs of the patient, as the gel started to release insulin in less than 1 h and prolonged up to 48 h.[43] Often it was seen that as a frequent side effect, hypoglycemia was caused due to a rapid release of insulin from drug delivery systems. Herein, the developed insulin–gel composite could uphold the release of insulin for a long period of time (two days) and subsequently would reduce the chances of hypoglycemia. Although the existing results are based on in vitro studies, their characteristics for self-regulated insulin delivery could be very significant for hyperglycemic treatment.

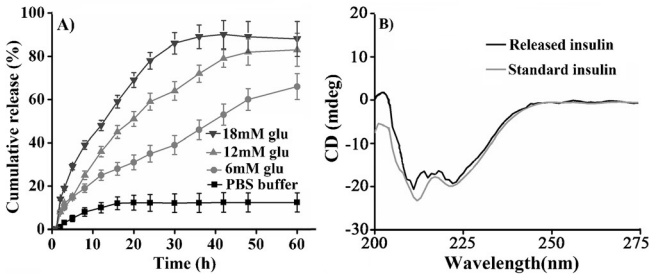

Figure 7. A) Cumulative release percentage of insulin. B) CD spectra of native and released insulin.

Circular dichroism (CD) study of insulin

Generally, native insulin exhibits two negative bands at $\lambda = 209$ and 223 nm in the CD spectra. These were referred to the α- and β-helical structure of insulin, respectively (Figure 7B).[41,44] The ratio of the both bands ($[\Phi_{209}/\Phi_{223}]$) provides a qualitative measure of the overall conformation of insulin. In this case the $[\Phi_{209}/\Phi_{223}]$ values of native and released insulin were found to be almost similar (1.16 and 1.08, respectively). Thus, no significant conformational change took place for the released insulin from the hydrogel network compared to that of standard one.

Thixotropy and injectable behavior of the insulin-loaded hydrogel

A simple time-dependent step-strain experiment was executed to look into the thixotropic behavior of the insulin (0.138 mg mL^{-1}) loaded gel at its MGC (5 mg mL^{-1}). The applied angular frequency was fixed at 1 rad s^{-1} throughout the experiment. Initially, 0.1% strain were applied to the insulin–gel composite, at which the G' value showed a higher account than the G'' value indicating distinct gel characteristics (Figure 8A). The applied strain was then rapidly enhanced from 0.1 to 50% and kept static for approximately 150 seconds. It was found that the G' value drastically decreased to a very low value ($\approx$81 Pa), which even appears below the G'' value ($\approx$192 Pa). The immediate drop of the G' value below the G'' value confirms that the gel behavior was completely destroyed and sol behavior was prominent (Figure 8A). Finally, the high strain was removed and a constant strain of 0.1% was again applied to observe the gel recovery property. Encouragingly, the insulin–gel composite recovered about 98% of its stiffness within approximately 80 seconds, which indicated the gradual break down and fast recovery of the cross-linked SAFIN resulting in sol-to-gel transition (Figure S9 in the Supporting Information). Furthermore, the same self-recovery experiment was performed four times in a cycle and in each case the stiffness was recovered about 95% within a time interval of approximately 80–110 seconds. Thus, the gel showed a distinct thixotropic property, which can be successfully modulated by altering the applied strain on the soft nanocomposite.

This thixotropic property of the insulin–gel composite made it suitable to be utilized as an injectable material.[24] To demonstrate the injectable behavior of the soft nanocomposite, we prepared the insulin-loaded hydrogel **1a** at pH 7.4 directly in a syringe (Figure 8B). The plunger was then pressed and the insulin–gel nanocomposite started flowing through the needle (Figure 8C). The solution was then collected in a glass vial (Fig-

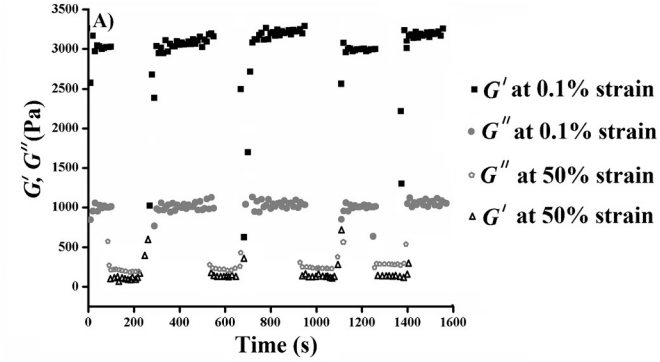

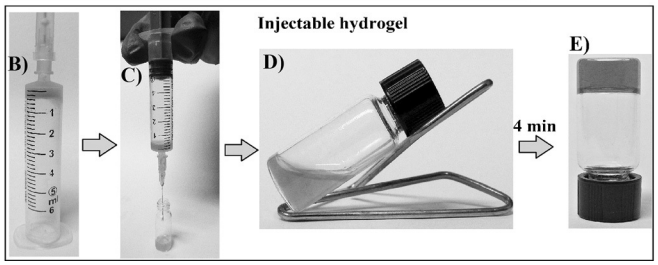

Figure 8. A) Time-dependent repetitive cycle of the step-strain analysis of the insulin-loaded hydrogel **1 a** with 5 mg mL^{-1} gelator concentration. Photographs of B) the insulin-incorporated hydrogel of **1 a** in a syringe, C) the insulin–gel composite flowing through the needle of a syringe, D) a solution of the insulin–gel composite after syringe processing, and E) the insulin-loaded hydrogel **1 a**.

ure 8 D) and turned into a gel within a very short time of approximately 4 min (Figure 8 E). Thus, the developed soft insulin–gel composite has immense potential as an injectable substance in diverse biomedicinal applications.

Cell viability study

Hydrogel **1 a** would find practical relevance in future applications if it shows considerable biocompatibility towards mammalian cells. Thus, we investigated the cell viability of compound **1 a** towards a human cell line, that is, HeLa cells, by a MTT-based assay.[47] A gelator solution in PBS (pH 7.4) at a concentration range of 5–200 μg mL^{-1} was incubated with HeLa cells. The hydrogelator **1 a** showed significant cell viability after an incubation period of 24 h. At a gelator concentration of 5 μg mL^{-1}, more than 94% of the cells were found alive (Figure 9). At a gelator concentration of 10 μg mL^{-1}, the cell viability was also noted to be 94%, which merely reduced to 90% upon increasing the concentration of compound **1 a** to 50 μg mL^{-1}. At moderately higher concentration of compound **1 a** (100 and 200 μg mL^{-1}), 90 and 88% cell viability were observed, respectively. Even at very high concentration of compound **1 a**, that is, 2000 μg mL^{-1} (that can be highest achieved without disconcerting the stability of the cell culture media), 85% of the cells were found to be alive. The biocompatibility was further tested by using the LIVE/DEAD viability kit for mammalian cells.[47,48] The exclusive presence of only a green fluorescence (excitation filter of BP460-495 nm and a band absorbance filter covering wavelengths below $\lambda = 505$ nm) ensuing from the enhanced fluorescence of DNA-intercalated calcein indicated the existence of live cells in the presence of compound **1 a** (200 μg mL^{-1}, Figure S10 in the Supporting Information). Furthermore, when the images were taken by using the excitation filter BP530-550 nm and a band absorbance filter covering wavelengths below $\lambda = 570$ nm, negligible red fluorescence was evinced. This result further confirmed the abundance of live cells and reduces the possibility of gelator-induced toxicity to mammalian cells. Hence, the newly developed LMHG **1 a** is inferred to be adequately cell viable.

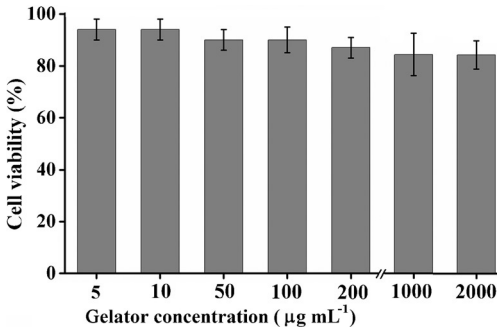

Figure 9. MTT-based % cell viability of HeLa cells with varying concentration of hydrogelator **1 a** (the incubation period was 24 h).

Conclusion

In summary, a pyrene-based PBA-containing injectable LMHG was developed and utilized to detect minute amounts of glucose through fluorescence sensing at physiological pH. Importantly, glucose-stimulated swelling of the hydrogel facilitated in vitro controlled release of entrapped insulin. Encouragingly, the gelators showed sufficient cell viability towards mammalian HeLa cells. Hence, the LMHG was employed in glucose sensing as well as glycol-sensitive insulin release at physiological pH. The stimuli-sensitive LMHG will have notable importance in the development of insulin regulatory systems required for diabetic therapies.

Experimental Section

Materials: L-Phenylalanine, *tert*-butyloxycarbonyl (Boc) anhydride, dicyclohexylcarbodiimide (DCC), 4-*N*,*N*-(dimethyl)aminopyridine (DMAP), 1-hydroxybenzotriazole (HOBT), *N*-hydroxysuccinimide (NHS), 4-carboxyphenylboronic acid, and solvents were procured from SRL, India. Trifluoroacetic acid (TFA) and sodium hydroxide (NaOH) were procured from Spectrochem, India. Pyrenebutyric acid and 2,2′-(ethylenedioxy)bis(ethylamine) were bought from Sigma. All deuterated solvents for NMR and FTIR spectroscopic experiments and 3-(4,5-dimethyl-2-thiazolyl)-2,5-diphenyl-2 *H*-tetrazolium bromide (MTT) were obtained from Sigma–Aldrich Chemical Co. Insulin (concentration = 40 IU mL^{-1}) was purchased from Torrent Pharmaceuticals Ltd. The LIVE/DEAD viability kit (l-3224) for mammalian cells used for the cell viability assays was procured from Molecular Probes, Invitrogen Chemical Company. High glucose Dulbecco's modified eagle medium (DMEM), heat-inactivated fetal bovine serum (FBS), and trypsin–ethylenediaminetetraacetic acid

(EDTA) (0.05%) were purchased from Invitrogen. Thin layer chromatography was done on Merck precoated silica gel 60-F_{254} plates.

^{1}H NMR spectra were recorded by using an AVANCE 500 MHz (Bruker) spectrometer. Mass spectrometric data were acquired by electron spray ionization technique on a Q-tof-micro quadruple mass spectrometer (Micromass). Elemental analyses were performed by using a Perkin–Elmer 2400 CHN analyzer. Transmission electron microscopy (TEM) images were taken on a JEOL JEM 2010 high-resolution microscope operating at 200 kV. Scanning electron microscopy (SEM) study was done on a JEOL-6700F microscope. A Perkin–Elmer Spectrum 100 FTIR Spectrometer was used to record the FTIR spectra. UV/Vis absorption spectra of the gelator **1a** and insulin were recorded on a Perkin–Elmer Lambda25 spectrophotometer..

Synthetic procedure: Gelators **1** and **1a** were synthesized by using the following method (Scheme S1 in the Supporting Information). Briefly, pyrene butyric acid (**i**) was coupled with the methyl ester of L-phenylalanine (**ii**) in dichloromethane by using DCC (1.1 equiv), a catalytic amount of DMAP, and HOBT (1.1 equiv) following the reported protocol. The coupled product **iii** was subjected to hydrolysis with 1 N NaOH solution followed by work up with 1 N HCl. The free acid terminal end of the L-amino acid **iv** was further coupled with mono Boc-protected 2,2′-(ethylenedioxy)bis-(ethylamine) to get the product **v**. Boc protection was removed by stirring the compound with TFA. The purified product **vi** was obtained by column chromatography by using 60–120 mesh silica gel and 10% methanol in chloroform. On the other hand, the NHS-linked 4-carboxyphenylboronic acid was prepared by using 4-carboxyphenylboronic acid, DCC (1.5 equiv), and NHS (1.1 equiv) in dry DMF (8 mL) and stirring overnight under a N_2 atmosphere. To this solution, an activated 4-carboxyphenylboronic acid mixture, compound **vi.** and dry pyridine were added. The solution was stirred overnight and the DMF was distilled out under vacuum. The residue mixture was then purified through column chromatography by using 100–200 mesh silica gel and methanol (3%)/chloroform as the eluent to obtain pure compound **1**. The terminal boronic acid was converted to the corresponding sodium salt (i.e., compound **1a**) by adding one equivalent 0.1 N NaOH (standardized) to the methanolic solution of the acid **1**. After brief stirring, the solvent was removed and lyophilized in Virtis4KBTXL-75 freeze drier under vacuum to get the sodium salt **1a**. ^{1}H NMR spectroscopic and mass spectrometric analysis of the gelators **1** and **1a** are provided in the Supporting Information.

Preparation of the hydrogel: The requisite amount of compound **1** was taken in a screw capped vial having an internal diameter (i.d.) of 10 mm and slowly heated to dissolve in aqueous buffer solutions of different pH values (i.e., pH 8.5–12). On the other hand, the gelation efficiency of compound **1a** was tested in PBS solution of pH 7.4. The solution was then allowed to cool slowly (undisturbed) to room temperature. The gelation was checked by "stable to inversion" of the aggregated material in the glass vial.

Determination of the gel-to-sol transition temperature (T_{gel}): The gel-to-sol transition temperature (T_{gel}) was recorded by gradually increasing the temperature (by using a rate of 2 °C min^{-1}) of the thermostatted oil bath in which the hydrogel-containing glass vial (i.d. 10 mm) was placed. The temperature (±0.5 °C) at which the gel liquefied and started to flow was referred to as T_{gel}.

Fluorescence spectroscopy: The emission spectra of the gelator at varying concentrations were recorded on a Varian Cary Eclipse luminescence spectrometer. Solutions were excited at $\lambda_{ex}=340$ nm in the absence and presence of glucose (0.1–1.2 mM). The excitation and emission slit width were both 5 nm.

Circular dichroism (CD) spectra: CD spectra of aqueous solutions of gelator **1a** and insulin were recorded with varying concentrations and varying the temperature in a quartz cuvette (1 mm path length) on a JASCO J-815 spectropolarimeter.

Measurement of the degree of swelling: To determine the swelling parameters, the xerogel (dry gel) of average weight of 5 mg was subjected to swell in aqueous PBS solution and glucose solutions of different concentrations from 6–18 mM. A piece of the xerogel was weighed and immersed in an excess of the swelling medium (PBS solution and glucose with different concentrations). At predetermined time intervals, the swollen gel was carefully removed from the medium and gently dried with a paper tissue in order to remove excess liquid. Subsequently, it was weighed very carefully until a constant mass was attained. Generally, the swollen gels are fragile in nature. Hence, they were kept on a grid boat with a mesh size of 1 mm. This process allowed the gel to be placed in water without hampering the stability. The percentage degree of swelling (% DS) was determined by using Equation (1). The % DS was plotted as a function of time.

To investigate the extent of dissolution during swelling, initially 1 mL of the PBS solution (pH 7.4) and the glucose solution (18 mM) were poured separately over 1 mL of the gel (prepared at its MGC of 5 mg mL^{-1}). These were kept undisturbed for 24 h. After filtration, fluorescence spectra of the supernatant solutions were observed at a certain time interval. The UV/Vis absorbance value of the supernatant solution was also recorded at $\lambda=340$ nm and the concentration of the dissolved compound **1a** was determined from the standard calibration curve. We have also analyzed the ^{1}H NMR spectra of the supernatant solution. Here D_2O was used as the gelation solvent and supernatant solution keeping the whole experimental procedure same.

Rheology: The rheological experiments were carried out in cone and plate geometry (diameter = 40 mm) on the rheometer plate by using an Anton Paar, MCR 302. The native gel was scooped on the rheometer plate so that there was no air gap with the cone. A frequency sweep experiment was done as a function of angular frequency (0.1–500 rad s^{-1}) at a fixed strain of 0.01% at 25 °C and the storage modulus (G') and the loss modulus (G'') were plotted against the angular frequency (ω).

Loading of insulin within hydrogel: For the preparation of an insulin-loaded hydrogel, the required amount of insulin (35–100 μL) (from 1.388 mg mL^{-1} or 40 IU mL^{-1} stock solution in saline water) was added to 1 mL of the gelator **1a** (5 mg mL^{-1}) in PBS solution (pH 7.4), and then the mixture was kept undisturbed until gel formation.

Release of entrapped insulin from hydrogel: Glucose solutions of different concentrations (6, 12, and 18 mM) were prepared in PBS solution of pH 7.4. These glucose solutions (600 μL) were added on top of the insulin (0.05 mg mL^{-1})–gel **1a** (5 mg mL^{-1}) composite and incubated for several hours. The supernatant solution was removed each time, and the amount of released material was estimated from the absorbance of insulin at $\lambda=276$ nm plotted in a standard calibration curve. The release rate was investigated in triplicates at room temperature and averaged.

Thixotropic property of the insulin-hydrogel composite: The continuous step-strain experiment was performed by first breaking the gel by application of a continuous strain of 0.1–50%. After the complete breakdown of the gel, as denoted by $G'' > G'$, gel recovery was attempted at a constant strain of 0.1%. The process was repeated to check the reversibility of the restoration process. The entire study was performed by keeping a constant angular frequency of 1 rad s^{-1}.

MTT assay: Cell viability of the hydorogelator was assessed by the microculture MTT reduction assay as previously reported.[49] The assay involves the conversion of a soluble tetrazolium salt by the mitochondrial dehydrogenase present in live cells to an insoluble colored product, that is, formazan. The amount of formazan formed is estimated spectrophotometrically after dissolution of the product in DMSO. The amount of formazan produced, is proportional to the number of live cells. The mammalian cells were seeded at a density of 15000 cells per well in a 96-well microtiter plate 18–24 h before the assay. A stock solution of the hydrogelator **1a** in PBS solution was prepared. The concentration of the gelator in the microtiter plate was varied from 5 to 200 $\mu g\,mL^{-1}$. The cells were incubated with the gelator for 24 h at 37 °C under 5% CO_2. The cells were further incubated for another four hours in 150 μL of the MTT stock solution (5 $mg\,mL^{-1}$). The produced formazan was dissolved in DMSO and the absorbance at $\lambda = 570$ nm was measured by using a BioTek Elisa Reader. The number of surviving cells was expressed as percent: viability = (A_{570}(treated cells) − background)/A_{570}(untreated cells) − background) × 100).

Fluorescence microscopic study: The LIVE/DEAD Viability/Cytotoxicity Kit for mammalian cells was used to examine the cell viability under a fluorescence microscope. The kit contains a mixture of two nucleic acid binding strains, calcein AM (component A) and ethidium homodimer-1 (component B). The acetomethoxy derivative of calcein (calcein AM) has the ability to pass through the cell membrane. The esterase enzyme present in live cells removes the acetoxy group. This form of the compound then intercalates with the DNA and resulted in an enhancement of fluorescence and a bright green color is observed. The ethidium homodimer-1 (EthD-1) can only pass through damaged cell membranes, thus it gets incorporated only into dead cells. It shows red fluorescence upon binding with DNA in dead cells. The kit was stored at −20 °C in the dark and was taken out and thawed at room temperature just prior to assay. An aliquot (4 μL) of the supplied 2 mM EthD-1 stock solution (component B) was added to 2 mL of sterile, tissue culture-grade PBS solution and the mixture was vortexed to ensure thorough mixing. An aliquot (1 μL) of the supplied 4 mM calcein AM stock solution (component A) was then added to the 2 mL EthD-1 solution and vortexed. The resulting working solution (2 μM calcein AM and 4 μM EthD-1) was then added directly to HeLa cells treated with the gelator solutions (200 $\mu g\,mL^{-1}$ for 24 h) and incubated further for 3 h. After incubation the excess dye was removed from the extracellular medium and the cells were washed with PBS solution. Then the cells were observed under the Olympus IX51 inverted microscope by using an excitation filter of BP460–495 nm and a band absorbance filter covering wavelengths below $\lambda =$ 505 nm and the excitation filter BP530–550 nm and a band absorbance filter covering wavelengths below $\lambda = 570$ nm.

Acknowledgements

P.K.D. is thankful to the Department of Science and Technology, India (SR/S1/OC-25/2011) for financial assistance. D.M., S.K.M., and M.G. acknowledge the Council of Scientific and Industrial Research, India for research fellowships.

Keywords: glucose · hydrogels · phenylboronic acid · self-assembly · sensors

[1] A. M. Lowman, M. Morishita, M. Kajita, T. Nagai, N. A. Peppas, *J. Pharm. Sci.* **1999**, *88*, 933 – 937.
[2] S. Vilaró, M. Palacín, P. F. Pilch, X. Testar, A. Zorzano, *Nature* **1989**, *342*, 798 – 800.
[3] R. Ma, L. Shi, *Polym. Chem.* **2014**, *5*, 1503 – 1518.
[4] D. Roy, B. S. Sumerlin, *ACS Macro Lett.* **2012**, *1*, 529 – 532.
[5] Y. Qiu, K. Park, *Adv. Drug Delivery Rev.* **2001**, *53*, 321 – 339.
[6] M. D. Segarra-Maset, V. J. Nebot, J. F. Miravet, B. Escuder, *Chem. Soc. Rev.* **2013**, *42*, 7086 – 7098.
[7] T. Miyata, T. Uragamia, K. Nakamae, *Adv. Drug Delivery Rev.* **2002**, *54*, 79 – 98.
[8] M. Ikeda, R. Ochia, I. Hamachi, *Lab. Chip* **2010**, *10*, 3325 – 3334.
[9] J. D. Decoppet, T. Moehl, S. S. Babkair, R. A. Alzubaydi, A. A. Ansari, S. S. Habib, S. M. Zakeeruddin, H. W. Schmidt, M. Grätzel, *J. Mater. Chem. A* **2014**, *2*, 15972 – 15977.
[10] J. Huang, C. L. Hastings, G. P. Duffy, H. M. Kelly, J. Raeburn, D. J. Adams, A. Heise, *Biomacromolecules* **2013**, *14*, 200 – 206.
[11] A. Bieser, J. Tiller, *Supramol. Chem.* **2008**, *20*, 363 – 367.
[12] T. D. James, K. R. A. S. Sandanayake, S. Shinkai, *Angew. Chem. Int. Ed. Engl.* **1996**, *35*, 1910 – 1922; *Angew. Chem.* **1996**, *108*, 2038 – 2050.
[13] S. Arimori, C. J. Ward, T. D. James, *Tetrahedron Lett.* **2002**, *43*, 303 – 305.
[14] Z. Wu, X. Zhang, H. Guo, C. Li, D. Yu, *J. Mater. Chem.* **2012**, *22*, 22788 – 22796.
[15] M. D. Phillips, T. M. Fyles, N. P. Barwell, T. D. James, *Chem. Commun.* **2009**, 6557 – 6559.
[16] Y. J. Huang, W. J. Ouyang, X. Wu, Z. Li, J. S. Fossey, T. D. James, Y. B. Jiang, *J. Am. Chem. Soc.* **2013**, *135*, 1700 – 1703.
[17] T. Hoeg-Jensen, S. Ridderberg, S. Havelund, L. Schäffer, P. Balschmidt, I. Jonassen, P. Vedsø, P. H. Olesen, J. Markussen, *J. Pept. Sci.* **2005**, *11*, 339 – 346.
[18] K. Kataoka, H. Miyazaki, M. Bunya, T. Okano, Y. Sakurai, *J. Am. Chem. Soc.* **1998**, *120*, 12694 – 12695.
[19] D. J. Abdallah, R. G. Weiss, *Adv. Mater.* **2000**, *12*, 1237 – 1247.
[20] V. Tharmaraj, K. Pitchumani, *RSC Adv.* **2013**, *3*, 11566 – 11570.
[21] A. M. Horgan, A. J. Marshall, S. J. Kew, K. E. S. Dean, C. D. Creasey, S. Kabilan, *Biosens. Bioelectron.* **2006**, *21*, 1838 – 1845.
[22] V. L. Alexeev, A. C. Sharma, A. V. Goponenko, S. Das, I. K. Lednev, C. S. Wilcox, D. N. Finegold, S. A. Asher, *Anal. Chem.* **2003**, *75*, 2316 – 2323.
[23] N. Javid, S. Roy, M. Zelzer, Z. Yang, J. Sefcik, R. V. Ulijn, *Biomacromolecules* **2013**, *14*, 4368 – 4376.
[24] S. K. Mandal, S. Brahmachari, P. K. Das, *ChemPlusChem* **2014**, *79*, 1733 – 1746.
[25] D. Mandal, T. Kar, P. K. Das, *Chem. Eur. J.* **2014**, *20*, 1349 – 1358.
[26] A. Bernet, M. Behr, R. Q. Albuquerque, M. Schmidt, J. Senker, H. W. Schmidt, *Prog. Colloid Polym. Sci.* **2013**, *140*, 1 – 13.
[27] J. Boekhoven, J. M. Poolman, C. Maity, F. Li, L. van der Mee, C. B. Minkenberg, E. Mendes, J. H. van Esch, R. Eelkema, *Nat. Chem.* **2013**, *5*, 433 – 437.
[28] S. K. M. Nalluri, N. Shivarova, A. L. Kanibolotsky, M. Zelzer, S. Gupta, P. W. J. M. Frederix, P. J. Skabara, H. Gleskova, R. V. Ulijn, *Langmuir* **2014**, *30*, 12429 – 12437.
[29] J. Raeburn, G. Pont, L. Chen, Y. Cesbron, R. LÃ©vy, D. J. Adams, *Soft Matter* **2012**, *8*, 1168 – 1174.
[30] V. J. Nebot, J. J. Ojeda-Flores, J. Smets, S. Fernndez-Prieto, B. Escuder, J. F. Miravet, *Chem. Eur. J.* **2014**, *20*, 14465 – 14472.
[31] J. M. Poolman, J. Boekhoven, A. Besselink, A. G. L. Olive, J. H. van Esch, R. Eelkema, *Nat. Protoc.* **2014**, *9*, 977 – 988.
[32] Z. Wu, S. Zhang, X. Zhang, S. Shu, T. Chu, D. Yu, *J. Pharm. Sci.* **2011**, *100*, 2278 – 2286.
[33] Y. Hirano, Y. Tokuoka, N. Kawashima, Y. Ozaki, *Vib. Spectrosc.* **2007**, *43*, 86 – 96.
[34] A. D'Urso, M. E. Fragala, R. Purrello, *Chem. Commun.* **2012**, *48*, 8165 – 8176.
[35] A. J. Tong, A. Yamauchi, T. Hayashita, Z. Y. Zhang, B. D. Smith, N. Teramae, *Anal. Chem.* **2001**, *73*, 1530 – 1536.
[36] J. Yan, G. Springsteen, S. Deeter, B. Wang, *Tetrahedron* **2004**, *60*, 11205 – 11209.
[37] A. Matsumoto, R. Yoshida, K. Kataoka, *Biomacromolecules* **2004**, *5*, 1038 – 1045.
[38] L. N. Neupane, C. R. Lohani, J. Kim, K. H. Lee, *Tetrahedron* **2013**, *69*, 11057 – 11063.
[39] E. Karadag, D. Saraydin, *Turk. J. Chem.* **2002**, *26*, 863 – 875.

[40] a) R. A. Siegel, Y. Gu, A. Baldi, B. Ziaie, *Macromol. Symp.* **2004**, *207*, 249 – 256; b) A. Shome, S. Debnath, P. K. Das, *Langmuir* **2008**, *24*, 4280 – 4288.
[41] S. Payyappilly, S. Dhara, S. Chattopadhyay, *J. Biomed. Mater. Res.* **2014**, *102*, 1500 – 1509.
[42] B. Yilmaz, Y. Kadioglu, *J. Pharmaceuticals* **2012**, *2*, 21 – 29.
[43] W. Wu, N. Mitra, E. C. Y. Yan, S. Zhou, *ACS Nano* **2010**, *4*, 4831 – 4839.
[44] L. Sun, X. Zhang, C. Zheng, Z. Wu, X. Xia, C. Li, *RSC Adv.* **2012**, *2*, 9904 – 9913.
[45] Q. Wu, L. Wang, H. Yu, J. Wang, Z. Chen, *Chem. Rev.* **2011**, *111*, 7855 – 7875.
[46] V. Lapeyre, I. Gosse, S. Chevreux, V. Ravaine, *Biomacromolecules* **2006**, *7*, 3356 – 3363.
[47] S. Brahmachari, D. Das, P. K. Das, *Chem. Commun.* **2010**, *46*, 8386 – 8388.
[48] M. Ghosh, S. Brahmachari, P. K. Das, *Macromol. Biosci.* **2014**, *14*, 1795 – 1806.
[49] M. B. Hansen, S. E. Nielsen, K. Berg, *J. Immunol. Methods* **1989**, *119*, 203 – 210.

Received: March 25, 2015
Revised: May 14, 2015
Published online on July 14, 2015